Unsaturated behavior of rammed earth: Experimentation towards numerical modelling

Parul Chauhan, Ahmad El Hajjar, Noémie Prime, Olivier Plé

Unsaturated behavior of rammed earth : experimentation towards numerical modelling

Parul Chauhan, Ahmad El Hajjar, Noémie Prime, Olivier Plé

Univ. Grenoble Alpes, Universite Savoie Mont Blanc, CNRS, LOCIE, 73000 Chambery, France

Abstract

This study concerns the coupled hydro-mechanical behavior of rammed earth, which is a real difficulty for the development of this construction technique. Unconfined compressive strength tests on samples conditioned at different relative humidities were performed to determine the variation of mechanical capacity with suction. Both compressive strength and Young's modulus increase with suction. Further, the effect of shear characteristics with the hydric conditions was studied by direct shear test. As suction induced cohesion contributes a significant part of strength, the apparent cohesion reduced with the reduction of suction. In addition, a considerable variation was observed in the friction angle. Unconsolidated undrained triaxial tests on unsaturated samples were performed to plot the failure envelope for a greater value of normal stress and to complete the failure envelope. These three test makes it possible to put in evidence a non-linearity in the failure envelope over all the suction range studied. Consolidated undrained triaxial tests on saturated samples were performed to determine the intrinsic cohesion and intrinsic friction angle. It was observed that Mohr-Coulomb criterion is not realistic for rammed earth and the failure envelope is non-linear for unsaturated con-

ditions. Thus, a failure criterion was proposed in which both cohesion and friction angle are dependent on normal stress applied. The expression for Bishop's effective stress for unsaturated soil was evaluated from the results of triaxial and unconfined compressive strength test together. The non-linear failure criterion obtained for a particular suction can be extended to other suction states through Bishop's effective stress formulation. It can further be used for coupled hydro-mechanical modeling of rammed earth structures.

Keywords: Rammed earth, suction, hydro-mechanical behavior, unsaturated state, constitutive modeling

---

1. Introduction

Rammed earth is a construction technique in which dense load-bearing walls are made by the dynamical compaction of moist sandy-loam soil in between removable shuttering or formworks. It represents a sound alternative to conventional construction techniques, from both energetic and mineral resources point of view and, thus, exactly fulfills the criteria for the urgent and intense ecological transitions needed for the sustainability of society. First, it has lower embodied energy than concrete or steel [1][2] (requires about 1% of energy needed for construction and transportation of concrete [3]), and therefore is responsible for much lower CO_2 emission. Besides, if not stabilized by a binding agent, is recyclable and then does not need mineral resources. In addition, it has been shown that it has desirable hydro-thermal regulator properties for the building in use [3][4][5]. Finally, this material appears to have resistance (around 1 to 2 MPa according to New Zealand standard NZS: 1998 [6] and New Mexico code, 2001 [7]) which is sufficient

for building few storey structures.

Despite these strong advantages concerning sustainability in the construction domain, raw earth suffers from a significant sensitivity to liquid water variation, which makes its use difficult to be generalized. Indeed, moisture ingress induces changes in the consistency of the earth (from solid to plastic), and decrease of the mechanical rigidity and capacity. This hydro-mechanical coupling is essential to be understood and quantified both for new construction and preservation of historical buildings and monuments, which are very relevant nowadays. This link between mechanical behavior and hydric conditions is better studied within the framework of unsaturated soil mechanics [8][9][10]. Hydro-mechanical coupling in rammed earth is more and more investigated thanks to experimental characterization [11][12][13][14][15][16][17] and numerical models proposed to reproduce these observations [18][19][20][21]. Indeed, various authors have already studied the influence of liquid water on the mechanical behavior of rammed earth, by considering suction as the governing internal stress variable in this unsaturated soil media. Jaquin et al. 2009 [11] analyzed the effect of suction on strength and stiffness characteristics through triaxial tests led on samples conditioned at different hydric states. They conclude that there is an increase in strength and stiffness with a decrease in water content (in the range of 5.5-10.2%). A ductile failure was observed for samples conditioned at low suction states, whereas a brittle failure was observed at high suction states. Bui et al. 2014 [13] investigated unconfined compressive strength and secant modulus test at a greater range of water content, from to 1-2% (dry state) to 11% (compaction water content). Below a water content of 4%,

no significant change in strength was observed. However, the compressive strength decreased from 2 to 0.1 MPa for water content increasing until 11%. This work thus identified, for the specific earth used, a critical hydric state regarding the mechanical capacity. Beckett et al. 2012 [22], from unconfined compressive strength under different varying suction and temperature conditions, concluded that suction is the predominant factor influencing strength.

In addition to increasing the strength, suction was also put in evidence to have an impact on other mechanical parameters. Champiré et al. 2016 [12], analyzed mechanical response under unload-reload cycles. At lower stress states, linear elasticity was observed, whereas at higher stress state residual plastic strains increased, at the same time than gradual degradation of stiffness, which is termed as damage. Further, both plastic strain and damage were dependent on the suction state. It was concluded that rammed earth exhibits a complex mechanical behavior which consists of elasto-plasticity and damage. Bui et al. 2014 [18], used Mazars's model to take into account this complex behavior. El Nabouch at al. 2018 [23], also highlighted the difference in the shear parameters between the core of the layers and their interface.

This study aims to investigate further the effect of suction on different mechanical parameters to define a constitutive hydro-mechanical model able to quantify the main features of the rammed earth material. For this purpose, we chose to adopt the concepts of unsaturated soil mechanics, in which many constitutive developments already exist and could be applied to our material. The work presented in this article gathers, in one hand, the presentation of a subsequent experimental campaign led at the material scale and on the

other hand analysis of the results of the hydro-mechanical tests which can be a step forward towards coupled modeling.

The first section is thus devoted to the description of the earth used in this work, and the manufacture of the samples, which are representative of the compacted structure element, and the hydric conditions applied.

The second section presents the extensive experimental campaign. The influence of suction was studied for unconfined compressive strength and Young's modulus determined through simple compression test, and shear parameters (cohesion and friction angle) analyzed through direct shear tests and unsaturated triaxial tests. These shear parameters are essential in soil mechanics, although very few studies about rammed earth focus on it. Higher values of normal stresses were applied on the triaxial test, which helps to obtain the failure envelope for a greater range of normal stress. Intrinsic shear parameters were evaluated by saturated triaxial tests. Based on this experimental analysis, the final section proposes a synthesis of these hydro-mechanical tests, which can help to obtain a coupled constitutive model able to predict the coupled behavior. Although our work is adapted for rammed earth construction, it is also suitable for other types of compacted earth technique.

2. Material and specimen preparation

2.1. Geotechnical characterization of the material

The material used in this study was procured from an existing construction site in the Auvergne-Rhone Alpes region of France. The particle size distribution of this earth shows that it contains 40% sand, 53% silt, and 7% clay. From figure 1, it is clear that the grain size distribution curve is

not enclosed within the spindle proposed by BS 1377-2:1990 [24]. The spindle provides a criterion to identify suitable soils for rammed earth constructions based on the shape of the particle size distribution. It is known that these specifications are often not followed by rammed earth and that, particle size distribution is not the determining parameter for selection of soil as rammed earth material. Some basic characterization tests for soil were performed. The Atterberg limit were evaluated as: liquid limit $w_l = 27.42\%$, plastic limit $w_p = 16.39\%$, giving a plasticity index defined as $I_p = w_l - w_p = 11.03\%$. According to the French Classification GTR (Guide de Terrassements Routier) for fine soils (more than 35 % of grains passing 80 µm and no grain size over 50 mm), it is low plastic silt ($I_p < 12\%$). In order to finely characterize the clay, the activity ($A_c = I_p/f$) where I_p is the plasticity index and f is the percentage of soil passing 2 µm sieve. The activity was found equal to 1.48, and is in the active range ($1.25 < A_c < 2.0$) and can be considered as slightly active. The cation exchange capacity (CEC) of 2.6 $cmol/kg$ and Specific surface area (S_{sp}) equal to $14.7 m^2/g$ were obtained. It suggests a very low percentage or absence of swelling clays (high S_{sp} and CEC).

2.2. Preparation of specimen

2.2.1. Compaction

In order to determine the water content to be added for optimum compaction, Standard Proctor test was done. A range of optimum moisture content (11.8 % to 13.4 %) to obtain maximum dry density was observed, and finally, optimum moisture content of 12.5 % was chosen for preparation of soil (figure 2). The earth was prepared at optimum moisture content and placed in an air-tight container for moisture homogenization.

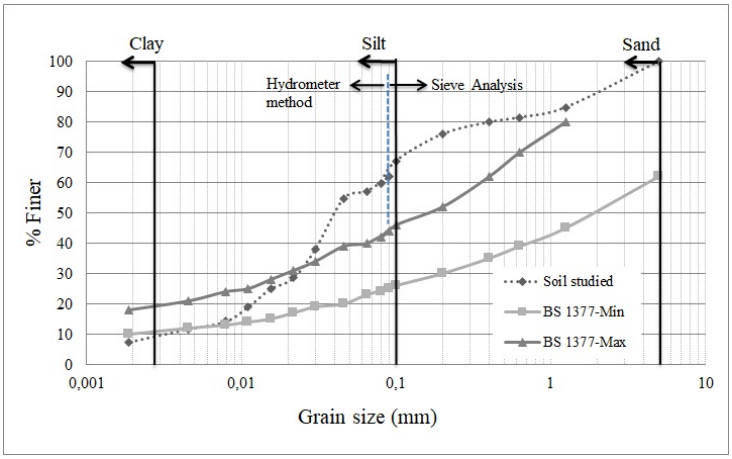

Figure 1: Grain size distribution and the guidelines by BS 1377 [24]

147

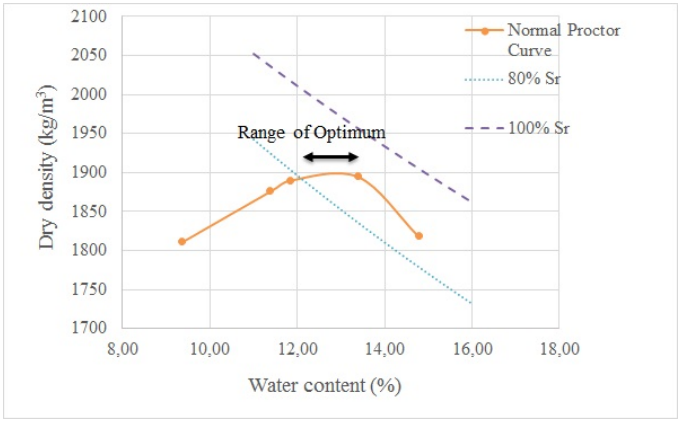

Figure 2: Results of Normal Proctor test

148 For the unconfined compressive strength (UCS) test, unconsolidated undrained
149 triaxial (in unsaturated state) and consolidated undrained triaxial (in satu-
150 rated state) test, 46 (21+21+4) cylindrical samples were prepared in a mold
151 which gives a diameter of 5cm and height of about 10cm. This gives a slen-
152 derness ratio of about 2. From the literature [25][26], it appears that for a

slenderness ratio of about 2, the compressive strength does not depend on the geometry, but on the method of compaction and the material. Here, a method of static double compaction was used for sample preparation. A compaction pressure of 5 MPa was chosen, as it is the standard pressure for Compressed Earth Blocs (CEB). Firstly, 80% of the total compaction pressure, i.e., 4MPa was applied gradually from one side, and then 100% of the total compaction pressure, i.e., 5MPa was applied from both sides, according to the methodology proposed by Bruno et al. 2015 [27]. This method gives a sample with more homogeneous density in contrast to the classical dynamic compaction method, where a gradient of density is observed, the layer of the earth being denser at top and looser at the bottom. Since in this study, the effect of suction is being analyzed on the mechanical properties, it is necessary to fix other influencing parameters. Using this method, there is better control of the compaction pressure, and the samples were produced with excellant repeatablity. The average dry density and the standard deviation from the average for each group of samples are shown in Table 1. These values lie within the range of dry density for earthen structures (1700 kg/m^3 to 2200 kg/m^3 [28]). Thus, even though the method of compaction differs from the actual method of compaction in the field, it is a material which is representative of rammed earth.

A similar method of double compaction with same compaction pressure of 5 MPa was used to prepare prismatic specimens for performing Direct shear tests (DST). A total of 63 [9 (samples at each suction state) x 7 (different suction conditions)] samples were prepared this way. A prismatic mold was used to obtain samples of size 60mm x 60mm x 30mm. Samples of these

dimensions were tested considering the mechanical capacity of the shear device.

It is important to note that the optimum moisture content depends on the method of compaction and energy imposed. The energy of compaction in the double compaction method is about 710 kJ/m^3, and for standard Proctor, the energy is about 569 kJ/m^3. The optimum water content obtained by standard Proctor is generally higher than required for rammed earth construction. Still, the dry density is the most important parameter influencing the strength properties [29] and the objective is to approach the dry density as in a rammed earth wall (dry density for rammed earth wall of the studied soil is about 1900 kg/m^3). Thus the optimum moisture content obtained from the standard Proctor can be used for the method of double compaction.

Table 1: Average dry density and standard deviation from the average for UCS, DST, and triaxial samples

Samples	Average dry density (kg/m^3)	Standard deviation (%)
UCS	1860	1.26
DST	1906	1.74
Triaxial	1910	0.36

2.2.2. Hydric Conditions and hygroscopic characterization

For the initial control of suction, liquid-vapor equilibrium method was used. The saturated aqueous solution of different salts (table 2) are used to control the relative humidity of the air around the samples by liquid-vapor

equilibrium. The exchange of water occurs in terms of water vapor based on Kelvin's thermodynamical equilibrium:

$$s = u_a - u_w = -\frac{\rho_w.R.T}{g.M_w} ln(RH) \tag{1}$$

Table 2: Different saline solutions and the relative humidity and corresponding suction imposed

Salt	KOH	CH_3CO_2K	$MgCl_2$	$NaBr$	$NaCl$	KCl	K_2SO_4
RH (%)	9	22.51	32.8	57.6	75.3	84.34	97.3
Suction (MPa)	331.3	205.3	153.4	75.9	39	23.4	3.8

where, s is the suction defined as difference of pore air pressure (u_a) and pore water pressure (u_w) at a given temperature T (in Kelvin, K), R is universal gas constant (R = 8.3143 J/mol/K), g is acceleration due to gravity, M_w is the molar mass of water ($M_w = 0.018Kg/mol$), ρ_w is the bulk density of water ($\rho_w = 1000Kg/m^3$) and RH is the relative humidity, which is defined as the ratio of partial vapor pressure P in the considered atmosphere and the saturation vapor pressure P_o at a particular temperature.

The suction equilibration of the 21 cylindrical specimens (for UCS test) is shown in the figure 3. The 21 samples were distributed in 7 different relative humidity boxes equilibrated at the following relative humidities 9%, 22.51%, 32.8%, 57.6%, 75.3%, 84.34% and 97.3% (see table 2) in group of 3 samples (similar method was used for unsaturated triaxial samples and direct shear samples). The samples were weighed regularly to follow the variation of water

content with time. Every time, the saturation of the saline solutions were checked, in order to ensure that samples equilibrate to the desired suction states. The equilibrium in the samples is supposed to be achieved when the variation of mass becomes less than 0.05% for more than 24 hours. The samples which were equilibrated at relative humidity less than 60% i.e., the ambient relative humidity for this region of France, the equilibration time was less than two weeks. For samples at a higher relative humidity (lower suction values), it took them more than a month for moisture balance. From the graph, it was seen that, samples equilibrated with $NaBr$ salt (RH = 57.6%) achieve a final water content which is less than the samples with $MgCl_2$ salt (RH = 32.8%), which is inconsistent considering that NaBr impose higher relative humidity than $MgCl_2$. The saturation of these solutions was checked at posteriori and was found that $MgCl_2$ saline solution was not saturated. Thus, it applies an unknown suction value. In the further sections, the results from this batch are not included (for results of UCS). Also, the samples placed in the K_2SO_4 box (RH = 97.3%, s = 3.8 MPa) are not fully equilibrated.

For saturated triaxial test, the samples after preparation by a similar method of double compaction and were placed inside an air-sealed plastic bag for a few days. The hydric state of these samples before testing was not essential to control since they will be first saturated before testing.

In order to obtain the soil-water retention curve (figure 4), 3 centimetric samples with dry mass ranging from 5g to 8g, were compacted by a similar method of double compaction. Firstly, the samples were air-dried at ambient conditions (temperature = $25°C$ and RH = 62%), then placed inside the oven at 70°C for sufficient duration of time (few days) until the mass was

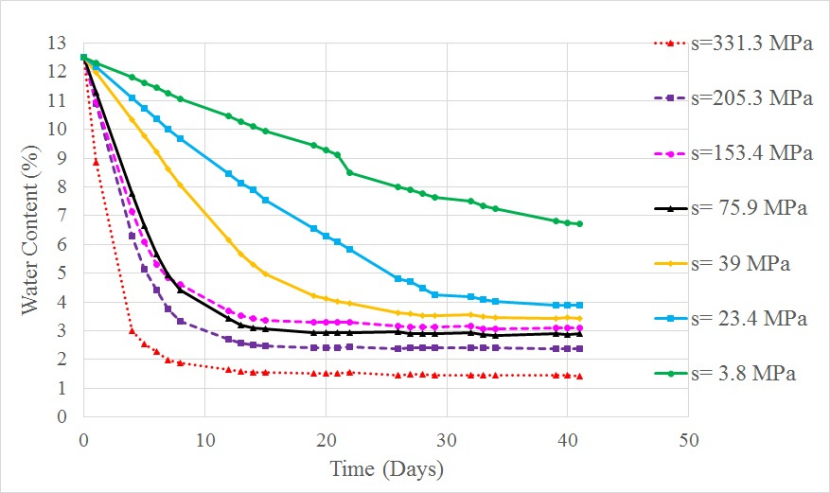

Figure 3: Moisture content variation with time during the suction equilibration in humidity controlled boxes for samples of UCS test directly placed in RH boxes after manufacture

stabilized. Then, the samples were placed in the KOH saline solution box with the lowest relative humidity (9%). When the samples were equilibrated i.e., mass variation is less than 0.05% in 24 hrs, they were transferred to the next higher relative humidity box. Points for sorption curve are obtained by this method. Once equilibrium was reached in the last box with the highest relative humidity (97.3%), the samples were again transferred towards lower relative humidity boxes. In this way, the points for the desorption curve are obtained. Hysteresis is observed in the soil water retention curve. A difference of 0.42 % volumetric water content at the maximum is observed which corresponds to a relative difference of around 10 %.

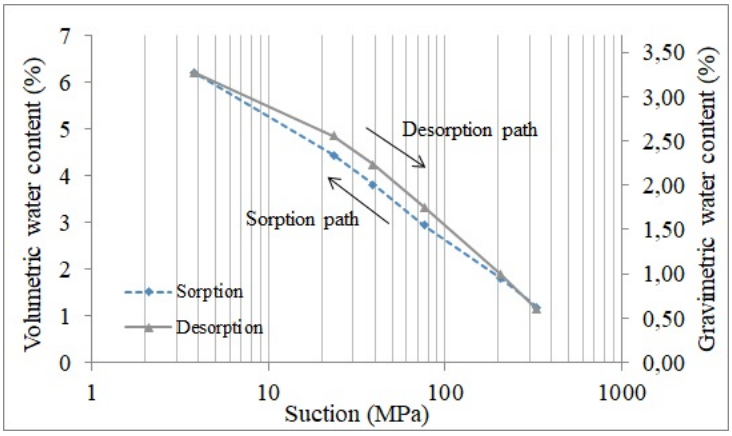

Figure 4: Soil-water retention curve showing both sorption and desorption path.

3. Apparent and intrinsic mechanical parameters

3.1. Influence of suction on apparent mechanical parameters

In this section, results from unconfined compressive strength (UCS) test, direct shear test (DST) and unsaturated triaxial test are presented to study the variation of parameters like UCS, initial tangent modulus, apparent cohesion and friction angle with suction. The analysis in these tests is done in terms of total stresses, whereas for the evaluation of the intrinsic parameters in the further section, the effective stress concept was used.

3.1.1. Unconfined compressive strength test

Unconfined Compressive strength (UCS) test was performed on the 21 samples. The samples were compressed with strain control at the rate of 0.005 mm/s to remain in quasi-static condition. As a global trend of the variation of UCS with suction, it can be seen on figure 5a that, the compressive strength decreases significantly with the decrease of suction. The

UCS value varies from 1.8 MPa to 6.7 MPa for suction increasing from 3.8 MPa to 331.3 MPa. It can be related to the gain of resistance of the earth structures in a building from the date of manufacture (corresponding to a water content of around 11-13%) up to a long time state, after several weeks of drying (with a water content of about 2 %). Inversely, this can also be related to the loss of mechanical strength for unusual water entry in the material. Firstly, 2 samples from a batch were compressed to obtain the compressive strength. Then, 1 out of every 3 samples (represented as triangular marking) from the batch, was compressed with unload-reload cycles in order to obtain Young's modulus. The unload-reload cycles were done at 30%, 60%, and 90% of the average compressive strength of the previous two samples. Still, the point of unloading cannot be stated surely as the compressive strength increased with cycles. These samples have higher compressive strength (about 30-40% higher) compared to the average strength of samples at the same suction tested without unload-reload cycles. It can be due to the additional compaction of the rammed earth samples during unloading-reloading and consequently a higher density state. The compressive strength observed at the ambient relative humidity of around 60% for European latitude was around 3 MPa. This value is consistent with what was observed in the literature [30].

An example of a stress-strain curve along with the unload-reload cycles is shown in figure 6a for a sample conditioned at 84.34% relative humidity. The Initial tangent modulus (E_{tan}) was evaluated from the initial slope of the stress-strain curve. The variation of the initial tangent modulus (expressed as the average of 3 tests at the same suction) with suction is shown in figure

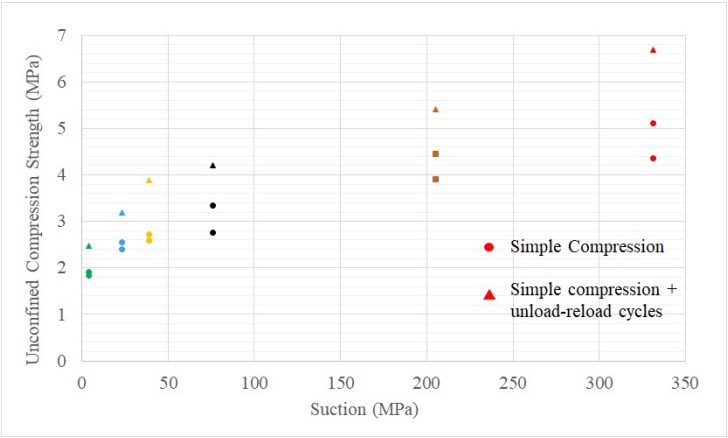

(a) Variation of compressive strength with suction, samples compressed with unload-reload cycles shown with triangular marking

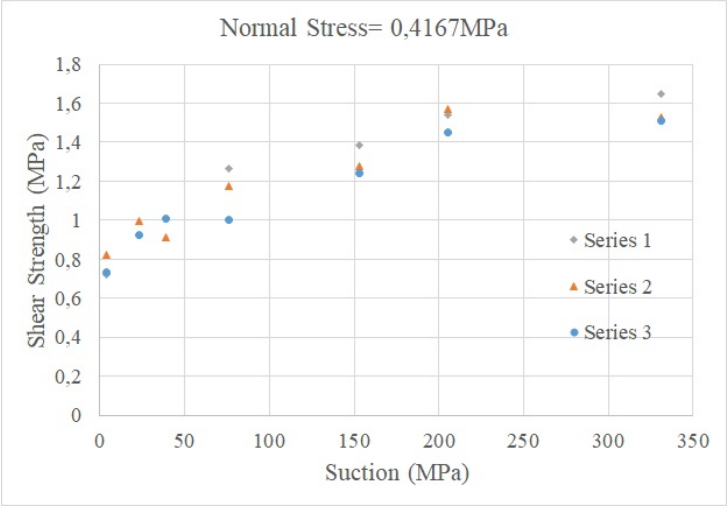

(b) Variation of Shear strength with suction at a constant normal stress

Figure 5: Influence of suction on UCS and shear strength

6b. A significant effect is observed with a decrease in suction. This behavior is also consistent with the literature [13][12][21]. The trend is similar to the variation of the compressive strength. The initial Young's modulus decreases almost 3 times as the suction reduces from 331.3 MPa to 3.8 MPa.

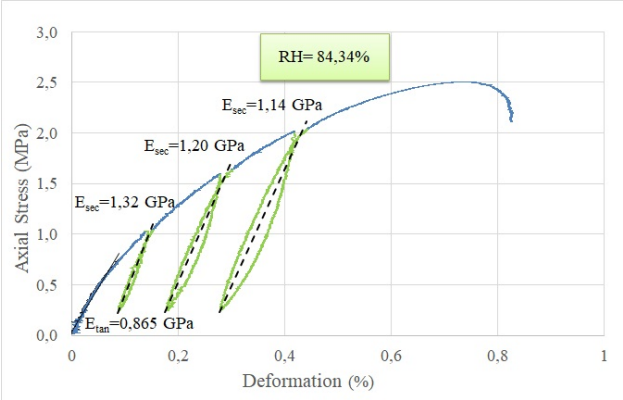

(a) Determination of Inital tangent modulus E_{tan} and Secant modulus E_{sec} for one test at RH= 84.34%, s= 23.4 MPa

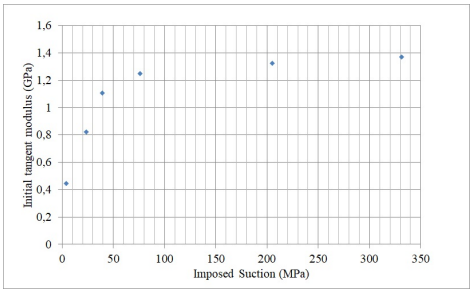

(b) Variation of E_{tan} with suction conditions

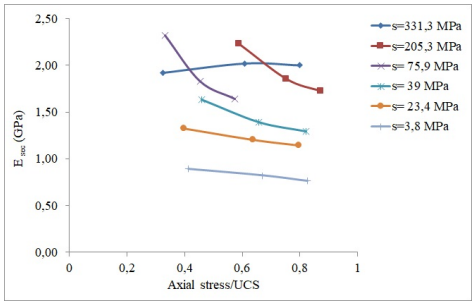

(c) Variation of E_{sec} with Axial stress to UCS ratio for different suction conditions

Figure 6: Results of Unconfined compressive strength test

The evolution of secant modulus (E_{sec}) with the ratio of maximum axial stress previously experienced to the UCS value is shown in figure 6c. A gradual reduction of the secant modulus i.e., damage, with an increase in axial stress, is observed in all the samples (except the sample conditioned at 331.3 MPa suction). This damage is dependent on the suction state, which is evident from the change in slope and increases with suction. The stiffness degradation varies from 22 % at 205.3 MPa suction to 13 % at 3.8 MPa suction.

3.1.2. Direct shear tests

In this study, an effort was made to enrich the classical building material approach in which only compressive strength and rigidity of the material are classically determined, we chose to investigate mechanical parameters which are more able to describe the strength properties of this unstabilized unsaturated soil: i.e. cohesion and friction angle, which are essential parameters in soil mechanics. Direct shear tests were thus conducted to determine the parameters of soil such as c and ϕ. Rammed earth is a construction material, but here is being analyzed as an unsaturated compacted soil. To correctly describe it, we thus need to determine its cohesion and friction angle, and quantify the effect of the suction state on these parameters.

Very few studies focus on the shear parameters of rammed earth [18][31][32] and none on the influence of hydric conditions on these parameters. So, in the present work, direct shear tests were conducted on different conditioning relative humidities to determine the variation of c and ϕ with suction. In this regard, 3 series of 21 samples each were subjected to the shear test. The series differ in the normal stress value applied (table 3) varying from 0.139 to 0.556 MPa. These values were chosen as traditional rammed earth wall are loaded by stresses of 0.1 - 0.3 MPa at the wall base [30].

Direct shear tests were conducted on these samples at a shear rate of $1mm/min$ with the automatic acquisition of both shear force and shear displacement every second. A shear stress-deformation curve for 3 tests at a relative humidity of 32.8% (Series 3) is shown in figure 7a. The shear modulus

Table 3: Normal load and stress applied in various series for a particular suction state

Load (kg)	Normal stress (MPa)	Series 1	Series 2	Series 3
5	0.139	o	*	+
10	0.278	o		+
15	0.417	o	*	+
20	0.556		*	

for all 3 samples sheared at different normal stress shows a low discrepancy, as it was observed for the majority of the tests. There is a brittle failure upon attaining the shear strength. In this test, there is no control over the drainage conditions and no mechanism to measure the pore pressure, but it is a quick test, so we suppose that suction does not vary significantly. Using the shear strength and normal stress, Mohr-coulomb envelope can be drawn in order to evaluate the apparent values of both cohesion and friction angle (figure 7b).

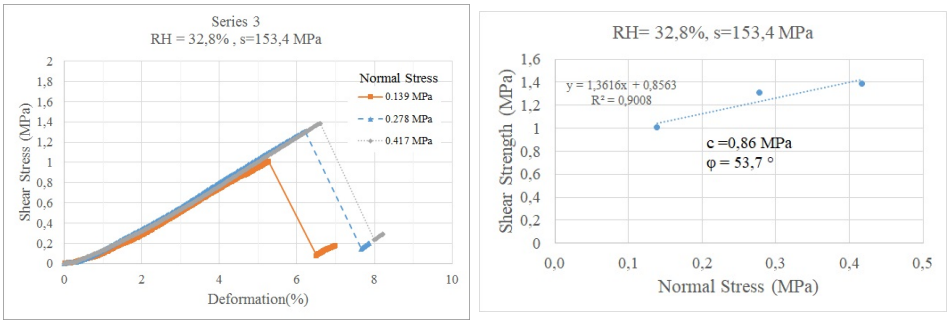

(a) Shear stress-shear strain curve

(b) Mohr-Coulomb envelope

Figure 7: Direct Shear Test result for Series 3 (s=153.4 MPa, RH = 32.8%)

For each suction state, 3 series (3 samples for each series) have been

tested, i.e., 9 samples (table 3). Each series gives a value of apparent cohesion and friction angle. The variation of cohesion and friction angle with imposed suction conditions is shown in figure 8 a and 8 b respectively, along with error bars expressed as the standard deviation of 3 results for different series. The cohesion of the samples increases with suction, which is justifiable from the theory of generalized effective stress, as there is an additional capillary cohesion induced by the partial saturation of the earth, which contributes a significant part of the shear strength. It can be seen that there is a lower standard deviation for higher relative humidities. This was also observed in the unconfined compression strength test (figure 5). This can probably be explained by the fact that a dry state of the material induces a fragile behavior. In consequence, the failure is more localized and thus is affected by small defaults in the matter, and its random distribution is responsible for a dispersion of the strength results. On the contrary, wetter samples are ductile, which induces a plastic failure concerning the global mass of the material. In this case, defaults have less influence, and the results present lower discrepancy. There is also a significant variation observed for the friction angle which varies from 43° to 63° when suction varies from 3.8 MPa to 331.3 MPa.

In figure 5b , shear strength is plotted against suction at constant normal stress. It can be observed that the rate of increase of shear strength with suction is very high at the lower suction, and this rate tends to decrease as we approach higher suction values. The explanation of this behavior can be found in literature [33][34][35]. Vanapalli et al. [33] compared the shear strength behavior with the soil water retention curve (figure 9). There is a

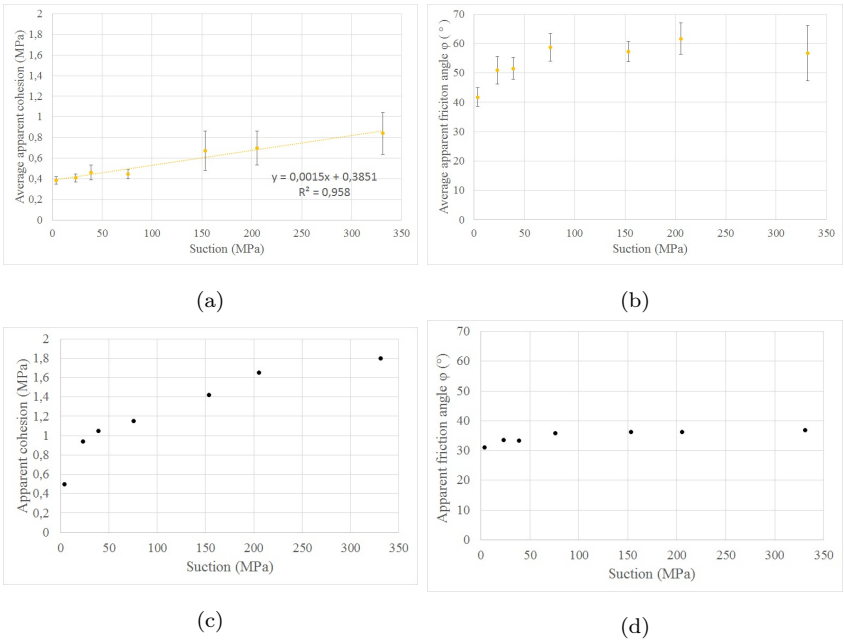

Figure 8: Variation of apparent shear parameters from direct shear tests with 3 results for each suction state (a and b) and unsaturated triaxial test with 1 result for each suction state (c and d)

linear increase of shear strength up to the air-entry value of suction. Further, there is a non-linear increase of shear strength up to the residual suction value and then depending on the soil, the strength may increase, decrease, or remain constant upon the increase in suction. On the one hand, for sand and silt water content at residual condition is very low, and it may not transmit suction effectively. Thus, even a substantial increase in suction will not increase shear strength. On the other hand, clay has well defined residual point and even at very high value of suction, there exists considerable water, which helps in effective transmission of suction, which leads to increase in strength. Since the soil in this study is predominantly sand and silt, at a higher value

of suction, the increase is less significant.

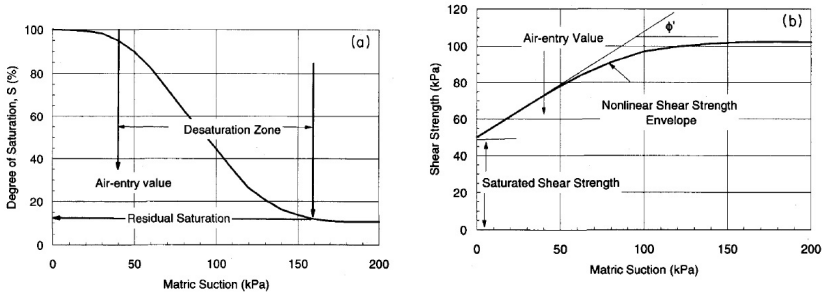

(a) Typical soil-water retention curve

(b) Shear Strength behaviour related to soil-water retention curve

Figure 9: Results of Vanapalli et al. 1996 [33]

3.1.3. Unsaturated triaxial tests

To confirm and complete the results, unsaturated triaxial tests were performed on 21 samples conditioned at 7 different suction states (relative humidity). For each suction suction state, 3 samples were tested at 3 different confining pressures (σ_3) i.e. 0.2 MPa, 1 MPa and 1.5 MPa. These values of σ_3 were chosen to plot the Mohr-Coulomb failure envelope at a higher range of normal stress as compared to the direct shear test to obtain the failure envelope at higher normal stresses. Also, the triaxial test has advantages such as there is no pre-defined failure surface during the test as in the direct shear test. For this reason, it is more representative of soil behavior. Using the 3 Mohr circles at each suction state, apparent values of cohesion (c) and friction angle (ϕ) were determined. The variation of c and ϕ as shown in figure 8 is similar to the one observed in the direct shear test. The cohesion value increases from 0.5 MPa to 1.8 MPa with suction, whereas there is no significant alteration in the friction angle (31° to 37°). It appears that values

of c and ϕ at a particular suction state are different for direct shear tests (done at lower normal stress) and unsaturated triaxial tests (done at higher normal stress). This behavior indicates that there is non-linearity in the failure envelope ($\tau - \sigma_n$ plane). This non-linearity will be further discussed in the further section.

Finally, figure 10 shows all the results obtained from UCS, DST, and UU triaxial test for 7 different suction states in $\tau - \sigma_n$ plane. It gives a global idea of the various tests performed and helps to plot the failure envelope at a higher range of normal stress.

3.2. Intrinsic shear parameters

In order to explain the effect of hydric state on these failure parameters, we need to investigate the intrinsic parameters c' and ϕ' which are independent of suction. CU saturated triaxial test was carried at 4 different confining pressures i.e. $\sigma_3 = 100$ kPa, 200 kPa, 300 kPa, and 1500 kPa along with the measurement of pore water pressure during the shearing (figure 11b). The samples were saturated by a method of stepped saturation. Before the saturation stage, it was made sure that air bubbles were removed from all the connections and pressure meters connected for the cell pressure and pore water pressure. After mounting the samples in the triaxial cell, a cell pressure increment of 100 kPa was applied, and the evolution of pore water pressure was monitored. The saturation of the sample was checked by Skempton's parameter $B = \Delta u/\Delta\sigma_3$, if B value was less than 0.95 (meaning that the sample is not yet saturated), the pore water pressure increased to maintain effective stress at 10 kPa. This low value of effective stress was chosen not to affect the soil structure. Further, the specimen saturation was rechecked

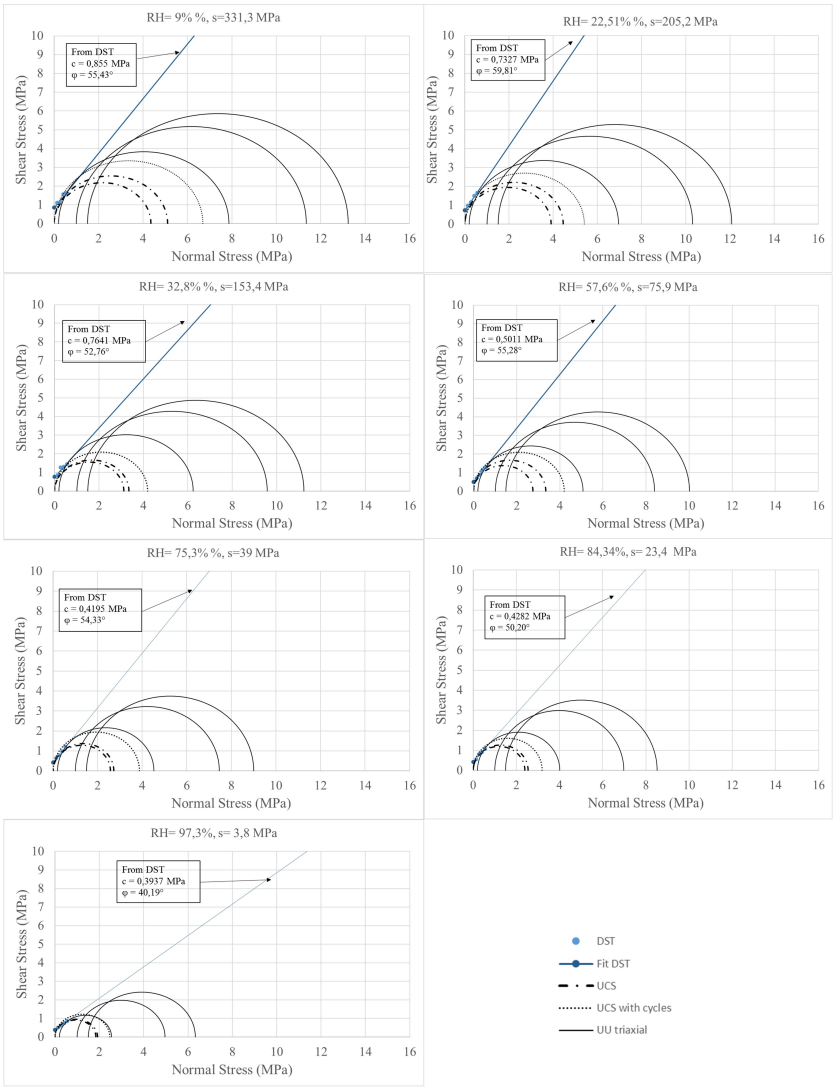

Figure 10: Results of DST, UCS and UU Triaxial test for all suction states

with the same procedure by raising the cell pressure by intervals of 100 kPa until reaching saturation. Typically, $B \geq 0.95$ confirm full specimen saturation. In the second stage, the sample was allowed to consolidate at different

confining pressures (σ'_3 = 100 kPa, 200 kPa, 300 kPa, and 1500 kPa). Finally, the sample was sheared at a displacement rate of 0.1428 mm/min [36] until failure. The results of these tests are shown in figure 12 in p'-q plane, where in the triaxial conditions p' and q are defined as:

$$p' = (\sigma'_1 + 2\sigma'_3)/3 \tag{2}$$

$$q = (\sigma'_1 - \sigma'_3) \tag{3}$$

A highly ductile failure was observed for all the samples (figure 11a), and according to ASTM D 4767-95 [36], the failure point is defined as the state of maximum effective stress obliquity i.e., maximum σ'_1/σ'_3. As the failure surface in p'-q and $\tau - \sigma$ plane represent the same failure state, the geometrical relation between these two allow us to compute the intrinsic parameters. The failure criteria in p'-q plane is defined as:

$$q = k + Mp' \tag{4}$$

with $M = 6sin\phi'/(3 - sin\phi')$ and $k = Mc'/tan\phi'$ From these equations, the effective parameters were evaluated as c' = 43.91 kPa and ϕ' = 32.53°, which are good from a soil mechanics point of view. These value obtained are similar to Gerard et al. 2015 [17], which is justifiable as the particle size distribution of both soil used is similar.

It is interesting to note that, the apparent cohesion at different suction state (from unsaturated triaxial) is significantly higher than the intrinsic cohesion (figure 8). However, the apparent friction angle values are quite similar to the intrinsic friction angle. This supports the fact that, with an increase in

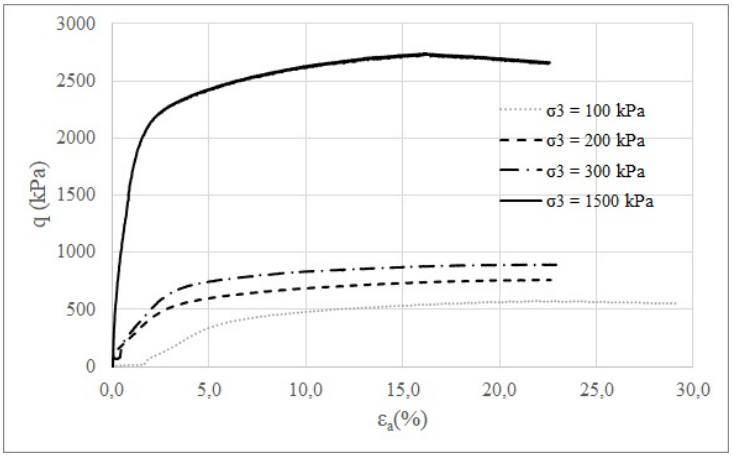

(a)

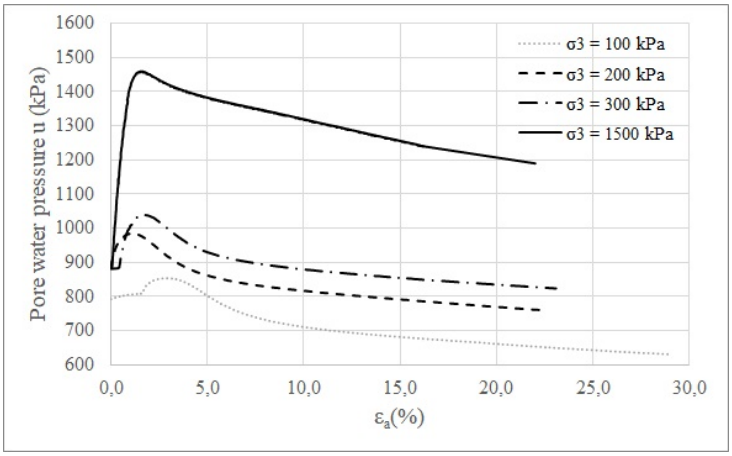

(b)

Figure 11: Variation of devaitoric stress (a) and pore water pressure (b) for 4 saturated samples at σ_3 = 100 kPa, 200 kPa, 300 kPa, and 1500 kPa

suction, the capillary induced cohesion increases and contributes a significant part to the strength. However, the part of shear strength that is due to friction between the particles does not vary so much as it is mostly dependent on the compaction state.

The comparison between the intrinsic and apparent (from direct shear test,

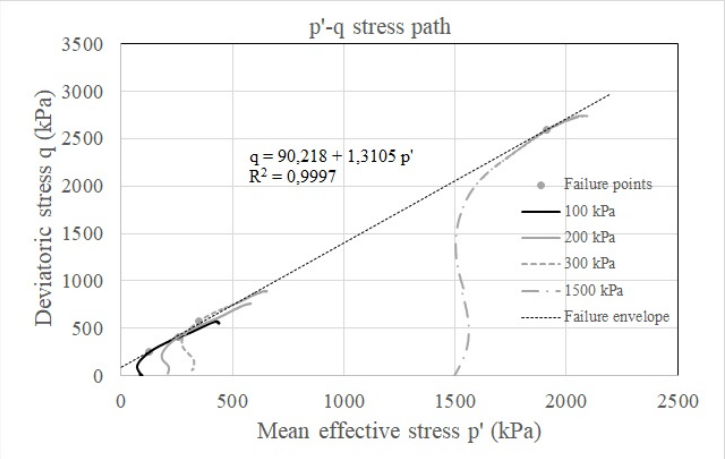

Figure 12: Failure envelope from 4 consolidated undrained triaxial test to determine intrinsic shear parameters

figure 8) shear parameters shows that c is significantly higher than c', which is due to the additional suction induced cohesion. ϕ is also higher than ϕ'. This is due to the fact that ϕ is evaluated in direct shear test at a normal stress range of 0.139 - 0.556 MPa. Due to the non-linearity in the Mohr-Coulomb failure envelope, the value of ϕ evaluated from the initial part of the curve is significantly higher.

4. Towards constitutive modeling

Linear Mohr-Coulomb failure criterion is the most common criterion for modeling the behavior of rammed earth and was used in different research [20][37][38] [21][30]. However, this model has various limitations. For an over-consolidated soil, the failure envelope is not a straight line but a curved line which is concave towards the normal stress axis [39][40][41]. Also, in the unsaturated samples due to higher confining stresses, the degree of saturation

can increase leading to change in consistency of the sample and affecting the behavior. Here, the linear Mohr-Coulomb failure envelope is not totally suitable in the case of rammed earth as the intrinsic mechanical behavior is changing. Moreover, it is essential to incorporate the role of suction and generalize the failure criteria as initially proposed by Gerard et al. 2015 [17]. To take into account the non-linearity of the failure envelope, we have used modified Mohr-Coulomb criteria according to Shen et al. [42], in which cohesion c and friction angle ϕ are described as a function of normal stress (σ_n). The expression for the shear strength remains the same, whereas c and ϕ are dependent on normal stress. The following functions were used to describe the shear parameters.

$$\phi = \phi_0(1 - \sqrt{\frac{\sigma_n}{2\sigma_c}}) \tag{5}$$

$$c = c_0 + (\sigma_c - c_0)\frac{\sigma_n}{2\sigma_c} \tag{6}$$

where, c_0 is apparent cohesion, ϕ_0 is apparent friction angle and σ_c is the critical confining pressure which is defined as the normal stress after which the shear strength does not increase. The non-linear Mohr-Coulomb failure envelope was plotted from Mohr circles for UCS and unsaturated triaxial tests. The parameter σ_c was adjusted for all the suction states to fit the data and is mentioned in table 4. From figure 13, the failure envelope is plotted for $s = 205.2$ MPa, $RH = 22.51\%$, parameter $\sigma_c = 6.5MPa$ is chosen to fit the data set. The values of c_0 and ϕ_0 are used from the direct shear tests. It is to be noted that, the results from UCS test performed with cycles are not used here. It is because, in reality, due to unload-reload cycles, higher

strength was observed and it is considered that it does not represent the same material.

Table 4: Values of the parameter σ_c corresponding to each suction state

Suction (MPa)	331.3	205.3	153.4	75.9	39	23.4	3.8
σ_c (MPa)	8.35	6.5	6.4	5.3	4.8	4.7	2.5

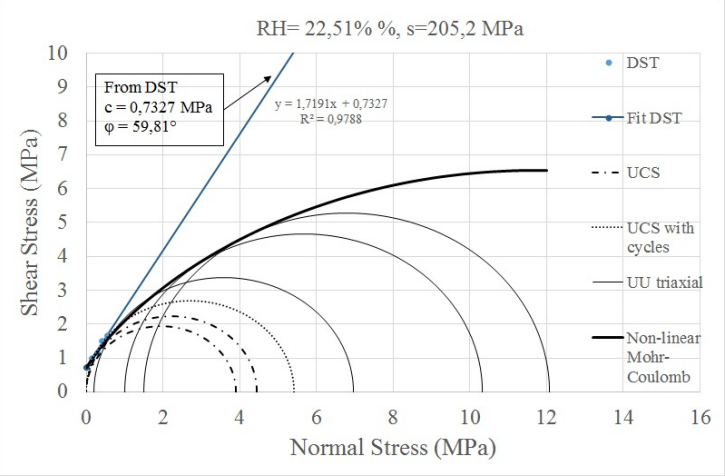

Figure 13: Non-linear failure envelope plotted for s =205.2 MPa and RH = 22.51 % using the results of UCS, DST and unsaturated triaxial test

In figure 14, the failure envelope for all the suction states is plotted. Here, we can observe its evolution with both normal stress and suction. The failure envelope from the saturated triaxial test has also been shown to observe the influence of the suction state on the failure envelope compared to the saturated state. This influence is represented by the vertical shift between the saturated triaxial criterion and unsaturated triaxial ones.

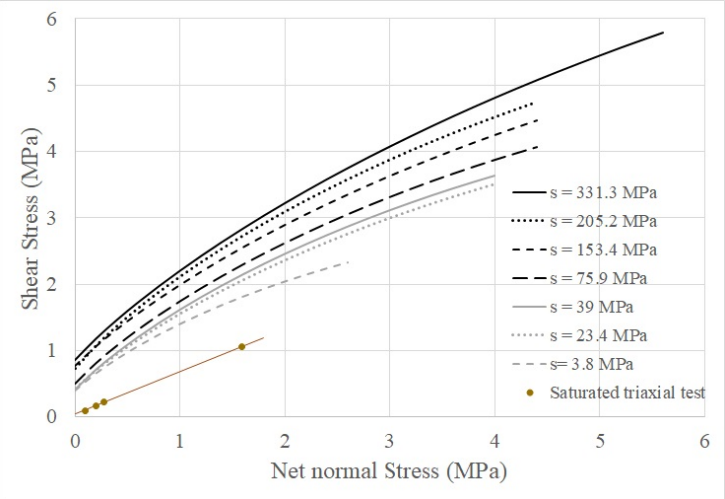

Figure 14: Failure envelope plotted for all suction states, where for the unsaturated states net normal stress $\sigma_n = \sigma - u_a$ and for the saturated state $\sigma_n = \sigma - u_w$

4.1. Generalised effective stress

The stress state variables represent the state of equilibrium of the system. For unsaturated soils, there are 2 different approaches to define the system and completely analyze the mechanical response. The first approach uses 2 independent stress state variables out of the 3 state variables for unsaturated soils i.e. net vertical stress $(\sigma - u_a)$, effective stress for saturated soils $(\sigma - u_w)$ and matric suction $(u_a - u_w)$. Commonly, $\sigma - u_a$ and $u_a - u_w$ are used. The second approach is generalized effective stress approach in which single effective stress defines the stress state of a multi-phase porous medium. The first approach allows to model behavior as a collapse for loose soil where only the suction variation can cause failure. Since we have a highly compacted soil, the generalized effective stress approach is more suitable. Here we use

Bishop's effective stress [43] :

$$\boldsymbol{\sigma'_{ij}} = \boldsymbol{\sigma_{ij}} + \chi s \delta_{ij} \tag{7}$$

where, $\boldsymbol{\sigma'_{ij}}$ is the effective stress tensor, $\boldsymbol{\sigma_{ij}}$ is the net stress tensor, s is the suction, δ_{ij} is the Kronecker delta(δ_{ij}=0 if $i \neq j$, else = 1) and χ is the effective stress parameter which is a function of degree of saturation.

To evaluate χ as a function of degree of saturation, first, we need to use the intrinsic shear parameters c' and ϕ' in the same approach as Gerard et al. [17]. According to Bishop 1960 [43], in the effective stress state reference, the normal stress shifts by an amount χs. It means that even for UCS test with $\sigma_3 = 0$, in effective stress reference it is being internally stressed by an amount χs. To evaluate χ, failure envelope from saturated triaxial is overlapped with Mohr circles from UCS and unsaturated triaxial test in effective stress reference.

Finally, χs is evaluated geometrically from figure 15 by using $\sigma'_3 = \chi s$ for UCS and $\sigma'_3 = \sigma_3 + \chi s$ for unsaturated triaxial test.

$$\chi s = \frac{r - c'.cos\phi'}{sin\phi'} - r - \sigma_3 \tag{8}$$

where $r = \frac{\sigma_1 - \sigma_3}{2}$ and $\sigma_3 = 0$ for UCS test. The value of χ was evaluated for each test and averaged (3 samples) for each suction state. It is plotted with the corresponding degree of saturation in log-log scale in figure 16. This gives the following relationship

$$log\chi = \alpha log S_r \tag{9}$$

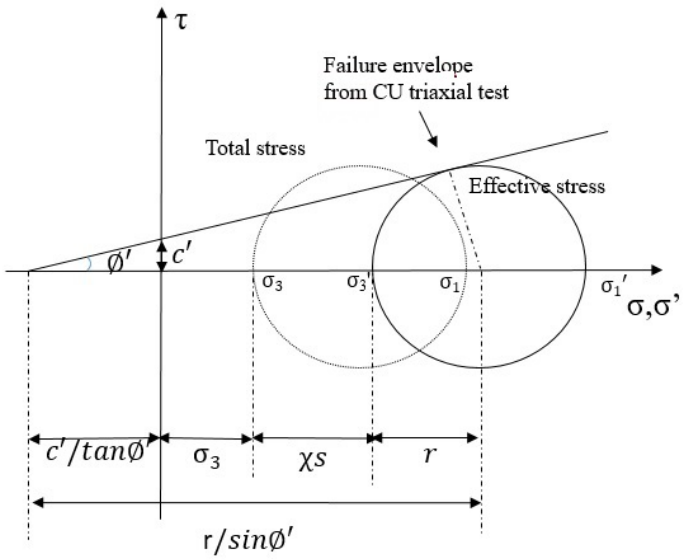

Figure 15: Determination of expression for χs using saturated triaxial test and mohr circles from unsaturated triaxial test and UCS ($\sigma_3 = 0$) using the methodology of Gerard et al .2015 [17]

$$\chi = (S_r)^{\alpha} \tag{10}$$

The value of α evaluated from this method is equal to 1.8802. This value is similar compared to Gerard et al. 2015 [17]. It can be justified from the fact the particle size distribution in both the studies are similar. The expression for Bishop's effective stress is written as:

$$\sigma'_{ij} = \sigma_{ij} + (S_r)^{1.8802} s\delta_{ij} \tag{11}$$

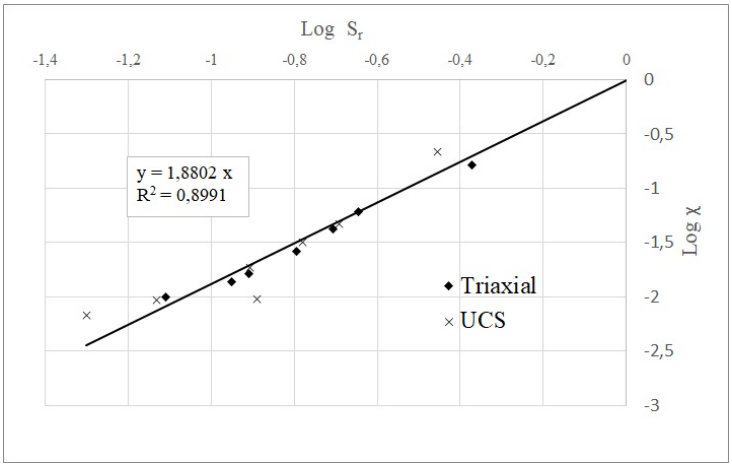

Figure 16: Determination of relation between χ and S_r

5. Conclusion

In the present study, a methodology to study the hydric influence on mechanical behavior is presented. The apparent mechanical parameters and intrinsic parameters were studied to provide a synthesis to define input parameters for a hydro-mechanical predictive model.

It has been proposed to work with more homogeneously compacted samples by a method of double compaction instead of the traditional method of dynamic compaction. Using this technique, the compaction pressure is better controlled, and samples are repeatable. Although this method differs from the actual method in the field, the dry density obtained is the range for traditional earth construction, and thus, is representative.

Matric suction is a state parameter which directly translates any hydric solicitation inside the material. The samples were conditioned to 7 different suction states using the method of liquid-vapor equilibrium before they were tested.

Unconfined compressive strength test was performed, with and without unload-reload cycles. The compressive strength and initial tangent modulus were found to increase with suction. Besides, it was found, that the compressive strength of samples which were compressed with unload-reload cycles was higher, indicating that the strength of rammed earth can still be improved by additional compaction.

Direct shear tests were performed with the same technique for sample preparation and control of hydric conditions. A brittle failure was observed upon attaining the shear strength. The shear modulus for samples sheared at different normal stress (but at same suction state) showed very less discrepancy.

Cohesion and friction angle were determined at different hydric state using the Mohr-coulomb envelope. The cohesion of the sample increased with suction, due to the presence of additional capillary cohesion, which is induced by the partial saturation. There was less deviation in the results for samples at lower suction states (wet state), where more ductile failure occurs. On the other hand, for samples at higher suction states (dry state), brittle failure occurred, which is more localized, and small defaults affected the results. A similar observation was found for results of UCS.

The apparent shear parameters were also evaluated with unsaturated triaxial test at 7 different suction states. The failure envelope, using this test, was plotted at a higher range of normal stress as compared to DST. It indicated that shear strength predicted from the Mohr-Coulomb criteria using DST is overestimated and in fact, the failure envelope is non-linear.This non-linearity was predominantly due to the unsaturated state of the samples rather than over-consolidation. Non-linearity was introduced in the shear strength equation by varying the cohesion and friction angle with normal stress. Finally, intrinsic shear parameters were determined using saturated triaxial test. By using the failure criterion in effective stress state reference and Mohr circles for UCS and unsaturated triaxial test, a log-log relation was observed between χ and S_r. It helped in calculating the effective stress parameter and thus, obtaining the Bishop's effective stress relationship.

By obtaining the global failure envelope and effective stress equation, it is a step-forward for coupled hydro-mechanical constitutive modeling of rammed earth, which can intrinsically introduce the effect of suction in the failure criterion. The future scope will be to estimate, for a given earth building

submitted to given hydric variations, whether the strains remain admissible, and if the resistance of the structure is sufficient or not.

6. Acknowledgment

We want to acknowledge ISTerre Grenoble and Chambery for the evaluation of Cation Exchange Capacity (CEC) and Specific surface area of our material.

References

[1] B. Little, T. Morton, Building with earth in scotland: Innovative design and sustainability, Scottish Executive Central Research Unit Edinburgh (2001).

[2] J. Morel, A. Mesbah, M. Oggero, P. Walker, Building houses with local materials: means to drastically reduce the environmental impact of construction, Building and Environment 36 (10) (2001) 1119–1126. doi:10.1016/s0360-1323(00)00054-8.

[3] D. Gallipoli, A. Bruno, C. Perlot, N. Salmon, Raw earth construction: is there a role for unsaturated soil mechanics, Proceedings of Unsaturated Soils: Research & Applications (2014) 55–62.

[4] D. Allinson, M. Hall, Hygrothermal analysis of a stabilised rammed earth test building in the uk, Energy and Buildings 42 (6) (2010) 845–852. doi:10.1016/j.enbuild.2009.12.005.

[5] C. Beckett, D. Ciancio, A review of the contribution of thermal mass to thermal comfort in rammed earth structures, ICSBE-2012: International Conference on Sustainable Built Environment (2012).

[6] S. N. Zealand, NZS 4297:1998 Engineering design of earth buildings 4297 (1998) 60.

[7] J. Tibbets, Emphasis on rammed earth—the rational, Interaméricas Adobe Builder 9 (2001) 4–33.

[8] A. Tarantino, A possible critical state framework for unsaturated compacted soils, Géotechnique 57 (4) (2007) 385–389. doi:10.1680/geot.2007.57.4.385.

[9] D. Toll, A framework for unsaturated soil behaviour, Géotechnique 40 (1) (1990) 31–44. doi:10.1680/geot.1990.40.1.31.

[10] D. Toll, B. Ong, Critical-state parameters for an unsaturated residual sandy clay., Géotechnique. 53 (1) (2003) 93–103. doi:10.1680/geot.53.1.93.37255.

[11] P. A. Jaquin, C. E. Augarde, D. Gallipoli, D. G. Toll, The strength of unstabilised rammed earth materials, Géotechnique 59 (5) (2009) 487–490. doi:10.1680/geot.2007.00129.

[12] F. Champiré, A. Fabbri, J. C. Morel, H. Wong, F. McGregor, Impact of relative humidity on the mechanical behavior of compacted earth as a building material, Construction and Building Materials 110 (2016) 70–78. doi:10.1016/j.conbuildmat.2016.01.027.

606 [13] Q. B. Bui, J. C. Morel, S. Hans, P. Walker, Effect of moisture content
607 on the mechanical characteristics of rammed earth, Construction and
608 Building Materials 54 (2014) 163–169. doi:10.1016/j.conbuildmat.
609 2013.12.067.

610 [14] P. A. Jaquin, C. E. Augarde, L. Legrand, Unsaturated characteristics of
611 rammed earth, Unsaturated Soils: Advances in Geo-Engineering (1995)
612 (2008) 417–422. doi:10.1201/9780203884430.ch53.

613 [15] E. Araldi, E. Vincens, A. Fabbri, J.-P. Plassiard, Identification of the
614 mechanical behaviour of rammed earth including water content in-
615 fluence, Materials and Structures 51 (4) (2018) 88. doi:10.1617/
616 s11527-018-1203-2.

617 [16] C. Beckett, C. Augarde, D. Easton, T. Easton, Strength characterisation
618 of soil-based construction materials., Géotechnique. 68 (5) (2018) 400–
619 409. doi:10.1680/jgeot.16.p.288.

620 [17] P. Gerard, M. Mahdad, A. Robert McCormack, B. François, A unified
621 failure criterion for unstabilized rammed earth materials upon varying
622 relative humidity conditions, Construction and Building Materials 95
623 (2015) 437–447. doi:10.1016/j.conbuildmat.2015.07.100.

624 [18] T. T. Bui, Q. B. Bui, A. Limam, S. Maximilien, Failure of rammed earth
625 walls: From observations to quantifications, Construction and Building
626 Materials 51 (2014) 295–302. doi:10.1016/j.conbuildmat.2013.10.
627 053.

[19] B. François, L. Palazon, P. Gerard, Structural behaviour of unstabilized rammed earth constructions submitted to hygroscopic conditions, Construction and Building Materials 155 (2017) 164–175. doi:10.1016/j.conbuildmat.2017.08.012.

[20] L. Miccoli, D. V. Oliveira, R. A. Silva, U. Müller, L. Schueremans, Static behaviour of rammed earth: experimental testing and finite element modelling, Materials and Structures 48 (10) (2015) 3443–3456. doi:10.1617/s11527-014-0411-7.

[21] H. Nowamooz, C. Chazallon, Finite element modelling of a rammed earth wall, Construction and Building Materials 25 (4) (2011) 2112–2121. doi:10.1016/j.conbuildmat.2010.11.021.

[22] C. Beckett, C. Augarde, The effect of relative humidity and temperature on the unconfined compressive strength of rammed earth (2012) 287–292doi:10.1007/978-3-642-31116-1_39.

[23] R. El-Nabouch, Q.-B. Bui, O. Plé, P. Perrotin, Characterizing the shear parameters of rammed earth material by using a full-scale direct shear box, Construction and Building Materials 171 (2018) 414–420. doi:10.1016/j.conbuildmat.2018.03.142.

[24] BS 1377: 1990—Methods of Test for Soils for Civil Engineering Purposes. British Standards Institute, London (1990).

[25] J.-E. Aubert, A. Fabbri, J. Morel, P. Maillard, An earth block with a compressive strength higher than 45 mpa!, Construction and Building

650 Materials 47 (2013) 366–369. doi:10.1016/j.conbuildmat.2013.05.
651 068.

652 [26] P. Walker, Characteristics of pressed earth blocks in compression, in:
653 Proceedings of the 11th international brick/block masonry conference,
654 Shanghai, China, 1997, pp. 14–16.

655 [27] A. W. Bruno, D. Gallipoli, N. Salmon, A. W. Bruno, D. Gallipoli,
656 J. Mendes, Briques de terre crue : procédure de compactage haute
657 pression et influence sur les propriétés mécaniques, 33èmes Rencon-
658 tres de l'AUGC, ISABTP/UPP, Anglet, 27 au 29 Mai 2015 (2015) 1–
659 9doi:hal-01167676.

660 [28] P. Walker, R. Keable, J. Martin, V. Maniatidis, Rammed earth: design
661 and construction guidelines, BRE Bookshop Watford, UK (2005).

662 [29] M. Olivier, Le matériau terre, compactage, comportement, application
663 aux structures en bloc sur terre, Ph.D. thesis, Lyon, INSA (1994).

664 [30] W. P. Maniatidis V, Structural capacity of rammed earth in compres-
665 sion, Journal of Materials in Civil Engineering 20 (3) (2008) 230–238.
666 doi:10.1061/(asce)0899-1561(2008)20:3(230).

667 [31] A. Corbin, C. Augarde, Investigation Into the Shear Behaviour of
668 Rammed Earth Using Shear Box Tests, First International Conference
669 On Bio-based Building Materials (2015) 93–98doi:10.1371/journal.
670 -pone.0018239.

671 [32] J. S. J. Cheah, P. Walker, A. Heath, T. K. K. B. Morgan, Evaluat-
672 ing shear test methods for stabilised rammed earth, Proceedings of the

673 Institution of Civil Engineers - Construction Materials 165 (6) (2012)
674 325–334. doi:10.1680/coma.10.00061.

675 [33] S. K. Vanapalli, D. G. Fredlund, D. E. Pufahl, A. W. Clifton, Model
676 for the prediction of shear strength with respect to soil suction, Cana-
677 dian Geotechnical Journal 33 (3) (1996) 379–392. arXiv:arXiv:1011.
678 1669v3, doi:10.1139/t96-060.

679 [34] J. K. M. Gan, D. G. Fredlund, H. Rahardjo, Determination of the shear
680 strength parameters of an unsaturated soil using the direct shear test,
681 Canadian Geotechnical Journal 25 (3) (1988) 500–510. doi:10.1139/
682 t88-055.

683 [35] D. G. Fredlund, A. Xing, M. D. Fredlund, S. L. Barbour, The re-
684 lationship of the unsaturated soil shear to the soil-water character-
685 istic curve, Canadian Geotechnical Journal 33 (3) (1996) 440–448.
686 doi:10.1139/t96-065.

687 [36] ASTM D 4767-95: Standard Test Method for Consolidated Undrained
688 Triaxial Compression Test for cohesive soils.

689 [37] L. Miccoli, A. Drougkas, U. Müller, In-plane behaviour of rammed earth
690 under cyclic loading: Experimental testing and finite element mod-
691 elling, Engineering Structures 125 (2016) 144–152. doi:10.1016/j.
692 engstruct.2016.07.010.

693 [38] T.-T. Bui, Q.-B. Bui, A. Limam, J.-C. Morel, Modeling rammed earth
694 wall using discrete element method, Continuum Mechanics and Thermo-
695 dynamics 28 (1-2) (2016) 523–538. doi:10.1007/s00161-015-0460-3.

[39] A. Bishop, D. Webb, P. Lewin, Undisturbed samples of london clay from the ashford common shaft: strength–effective stress relationships, Geotechnique 15 (1) (1965) 1–31. doi:10.1680/geot.1965.15.1.1.

[40] A. Penman, Shear characteristics of a saturated silt, measured in triaxial compression, Geotechnique 3 (8) (1953) 312–328. doi:10.1680/geot.1953.3.8.312.

[41] J. Atkinson, Stress path tests to measure soil strength parameters for shallow landslips, Proc. 11th ICSMFE, AA Balkema, Brookfield, VT, 1985 2 (1985) 983–986.

[42] B. Shen, J. Shi, N. Barton, Journal of Rock Mechanics and Geotechnical Engineering An approximate nonlinear modified Mohr-Coulomb shear strength criterion with critical state for intact rocks, Journal of Rock Mechanics and Geotechnical Engineering (4) (2018) 645–652. doi:10.1016/j.jrmge.2018.04.002.

[43] A. W. Bishop, The principal of effective stress, Norwegian Geotechnical Institute 32 (1960) 1–5.